VOLUME 35 | SUPPLEMENT 2 | MARCH 2022

MODERN PATHOLOGY

ABSTRACTS (1172–1186)

PEDIATRIC AND PERINATAL PATHOLOGY

2022

USCAP 111TH ANNUAL MEETING

REAL INTELLIGENCE

MARCH 19–24, 2022 LOS ANGELES, CALIFORNIA

Published by
SPRINGER NATURE
www.ModernPathology.org

USCAP Creating a Better Pathologist
AN OFFICIAL JOURNAL OF THE UNITED STATES AND CANADIAN ACADEMY OF PATHOLOGY

EDUCATION COMMITTEE

Rhonda K. Yantiss
Chair

Kristin C. Jensen
Chair, CME Subcommittee

Laura C. Collins
Chair, Interactive Microscopy Subcommittee

Yuri Fedoriw
Short Course Coordinator

Ilan Weinreb
Chair, Subcommittee for Unique Live Course Offerings

Carla L. Ellis
Chair, DEI Subcommittee

Adebowale J. Adeniran
Kimberly H. Allison
Sarah M. Dry
William C. Faquin
Karen J. Fritchie
Jennifer B. Gordetsky
Levon Katsakhyan, Pathologist-in-Training
Melinda J. Lerwill
M. Beatriz S. Lopes
Julia R. Naso, Pathologist-in-Training
Liron Pantanowitz
Carlos Parra-Herran
Rajiv M. Patel
Charles "Matt" Quick
David F. Schaeffer
Lynette M. Sholl
Olga K. Weinberg
Maria Westerhoff

ABSTRACT REVIEW BOARD

Benjamin Adam
Oyedele Adeyi
Mariam Priya Alexander
Daniela Allende
Catalina Amador
Vijayalakshmi Ananthanarayanan
Tatjana Antic
Manju Aron
Roberto Barrios
Gregory R. Bean
Govind Bhagat
Luis Zabala Blanco
Michael Bonert
Alain C. Borczuk
Tamar C. Brandler
Eric Jason Burks
Kelly J. Butnor
Sarah M. Calkins
Weibiao Cao
Wenqing (Wendy) Cao
Barbara Ann Centeno
Joanna SY Chan
Kung-Chao Chang
Hao Chen
Wei Chen
Yunn-Yi Chen
Sarah Chiang
Soo-Jin Cho
Shefali Chopra
Nicole A. Cipriani
Cecilia Clement
Claudiu Cotta
Jennifer A. Cotter
Sonika M. Dahiya
Elizabeth G. Demicco
Katie Dennis
Jasreman Dhillon
Anand S. Dighe
Bojana Djordjevic
Michelle R. Downes
Charles G. Eberhart
Andrew G. Evans
Fang Fan
Julie C. Fanburg-Smith
Gelareh Farshid
Michael Feely
Susan A. Fineberg
Dennis J. Firchau
Gregory A. Fishbein
Agnes B. Fogo
Andrew L. Folpe
Danielle Fortuna
Billie Fyfe-Kirschner
Zeina Ghorab
Giovanna A. Giannico
Anthony J. Gill
Tamar A. Giorgadze
Alessio Giubellino
Carolyn Glass
Carmen R. Gomez-Fernandez
Shunyou Gong
Purva Gopal
Abha Goyal
Christopher C. Griffith
Ian S. Hagemann
Gillian Leigh Hale
Suntrea TG Hammer
Malini Harigopal
Kammi J. Henriksen
Jonas J. Heymann
Carlo Vincent Hojilla
Aaron R. Huber
Jabed Iqbal
Shilpa Jain
Vickie Y. Jo
Ivy John
Dan Jones
Ridas Juskevicius
Meghan E. Kapp
Nora Katabi
Francesca Khani
Joseph D. Khoury
Benjamin Kipp
Veronica E. Klepeis
Christian A. Kunder
Stefano La Rosa
Stephen M. Lagana
Keith K. Lai
Goo Lee
Michael Lee
Vasiliki Leventaki
Madelyn Lew
Faqian Li
Ying Li
Chieh-Yu Lin
Mikhail Lisovsky
Lesley C. Lomo
Fang-I Lu
aDeqin Ma
Varsha Manucha
Rachel Angelica Mariani
Brock Aaron Martin
David S. McClintock
Anne M. Mills
Richard N. Mitchell
Hiroshi Miyamoto
Kristen E. Muller
Priya Nagarajan
Navneet Narula
Michiya Nishino
Maura O'Neil
Scott Roland Owens
Burcin Pehlivanoglu
Deniz Peker Barclift
Avani Anil Pendse
Andre Pinto
Susan Prendeville
Carlos N. Prieto Granada
Peter Pytel
Stephen S. Raab
Emilian V. Racila
Stanley J. Radio
Santiago Ramon Y Cajal
Kaaren K Reichard
Jordan P. Reynolds
Lisa M. Rooper
Andrew Eric Rosenberg
Ozlen Saglam
Ankur R. Sangoi
Kurt B. Schaberg
Qiuying (Judy) Shi
Wonwoo Shon
Pratibha S. Shukla
Gabriel Sica
Alexa Siddon
Anthony Sisk
Kalliopi P. Siziopikou
Stephanie Lynn Skala
Maxwell L. Smith
Isaac H. Solomon
Wei Song
Simona Stolnicu
Adrian Suarez
Paul E. Swanson
Benjamin Jack Swanson
Sara Szabo
Gary H. Tozbikian
Gulisa Turashvili
Andrew T. Turk
Efsevia Vakiani
Paul VanderLaan
Hanlin L. Wang
Stephen C. Ward
Kevin M. Waters
Jaclyn C. Watkins
Shi Wei
Hannah Y. Wen
Kwun Wah Wen
Kristy Wolniak
Deyin Xing
Ya Xu
Shaofeng N. Yan
Zhaohai Yang
Yunshin Albert Yeh
Huina Zhang
Xuchen Zhang
Bihong Zhao
Lei Zhao

To cite abstracts in this publication, please use the following format: **Author A, Author B, Author C, et al. Abstract title (abs#). In "File Title."** ***Modern Pathology*** **2022; 35 (suppl 2): page#**

1172 Pediatric Hepatic Vascular Tumors: Clinicopathologic Characterization of 32 Cases and Proposed Updates to Current Classification Schemes

Lara Berklite[1], Faizan Malik[1], Sarangarajan Ranganathan[1], Anita Gupta[2]
[1]Cincinnati Children's Hospital Medical Center, Cincinnati, OH, [2]Cincinnati Children's Hospital, Cincinnati, OH

Disclosures: Lara Berklite: None; Faizan Malik: None; Sarangarajan Ranganathan: None; Anita Gupta: None

Background: Pediatric hepatic vascular tumors (HVT) are rare neoplasms with pathologic features distinct from their cutaneous counterparts. Behavior ranges from benign to malignant with individual subtypes having therapeutic significance. Histopathologic descriptions of large cohorts are scarce in the literature.

Design: 32 putative HVTs diagnosed from 1970 to 2021 at a pediatric hospital were retrieved. All available clinical and pathologic material including immunohistochemical stains, was reviewed. Lesions were reclassified according to the current ISSVA and upcoming WHO classification of pediatric tumors.

Results: HVTs were classified as: hepatic congenital hemangioma (HCH; n=12), hepatic infantile hemangioma (HIH; n=11), hepatic angiosarcoma (HA; n=3), and hepatic epithelioid hemangioendothelioma (HEHE; n=1). Vascular malformations (n=4) or vascular dominant mesenchymal hamartoma (n=1) were excluded. Clinicopathologic features are summarized in Table 1. 11 HCH showed involutional features with calcification, necrosis, and hemorrhage with central larger vessels and small peripheral channels (Figure 1A). HCH was subtyped as rapidly involuting HCH (4/12), partially involuting HCH (7/12), and non-involuting HCH (1/12). HIH showed closely placed capillaries with some demonstrating anastomosing channels with plump, and focally piling endothelium ("redundancy"). A few HIHs showed worrisome features like solid, glomeruloid areas, increased mitoses, and epithelioid morphology with variable nuclear atypia suggesting aggressiveness (Figure 1B-D). All 3 HA had sheet-like and solid areas with 1 having glomeruloid foci (Figure 1E-F). The widely metastatic and fatal HEHE was from a 5-year-old male who had multiple liver lesions reaching up to 5 cm. The intraparenchymal HEHE showed infiltrative cords of mitotically active epithelioid cells with intracytoplasmic lumina. Immunohistochemically, all HIHs and HA were GLUT-1 positive. Limited follow-up information was available. 1 HIH patient died from post-operative complications, while 3 are alive without disease. 5 HCH patients are alive and well. 2/3 HA patients died due to disease and 1 patient is alive without recurrence.

Table 1. PEDIATRIC HEPATIC VASCULAR TUMORS

	Hepatic Congenital Hemangioma (n=12)	Hepatic Infantile Hemangioma (n = 11)	Hepatic Angiosarcoma (n =3)
CLINICOPATHOLOGIC FEATURES			
Age	Mean 8.5 months (n = 11) range 5 days – 60 months	Mean 14 months (n = 10) range 2 months – 48 months	Mean 26 months Range 7 – 48 months
Gender (M:F)	1:1 (n = 10)	1:1.5 (n = 10)	1:2
Tumor size (cm) by imaging	Mean 3.9 cm (n = 6) Range 1.6 – 6 cm	Mean 4.6 cm (n = 3)	Mean 9.4 cm Range (2 – 21 cm)
Specimen	Liver biopsy (1/11); resection (10/11)	Liver biopsy (n = 7), wedge resection (n =1), explant (n = 3)	Explant (2/3); liver biopsy (1/3)
Location	Subcapsular (5/12); Hilar (2/12); Lobe location: Left lobe (4/7), right lobe (3/7)	Subcapsular (4/7); intraparenchymal (3/7)	Multifocal parenchymal involvement (3/3)
Focality	Solitary (12/12)	Solitary (2/7); multifocal (5/7)	Multifocal (3/3)
Histological findings	Calcification (10/12); necrosis (10/12); EMH (10/12); Epithelioid / plump endothelium (8/12); intraluminal papillary proliferation (2/12);	Anastomosing vessels (5/11) with sinusoidal endothelial "redundancy" in (4/5); bland plump endothelium (4/11); focus of nuclear atypia/ nucleolar prominence (6/11); solid areas (1/11)	Epithelioid / plump endothelium (3/3); solid, sheet-like areas (3/3); epithelioid "glomeruloid" nodules (1/3); nuclear membrane irregularities and atypia (3/3); multiple nucleoli (1/3)
MITOTIC ACTIVITY			
≤2/10 hpf	8 / 11	11 / 12	0 / 3
>2 but ≤5/10 hpf	2 / 11	0 / 12	1 / 3
>5/10 hpf	1 / 11	1 / 12	2 / 3

Figure 1 - 1172

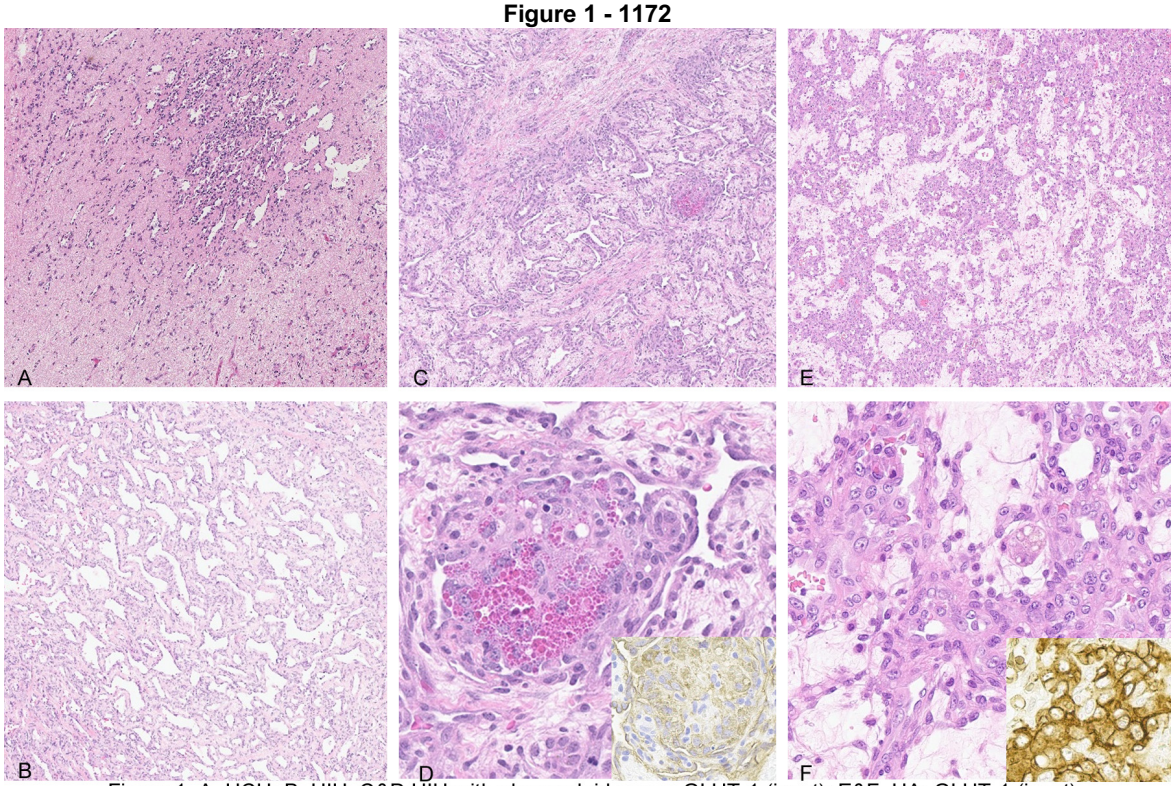

Figure 1. A. HCH; B. HIH; C&D HIH with glomeruloid areas; GLUT-1 (inset); E&F. HA; GLUT-1 (inset)

Conclusions: Our series highlights the diagnostic challenges of HVTs. To our knowledge, this is the largest series of pediatric HVTs which reviews clinicopathologic features based on the upcoming WHO / current ISSVA scheme. We propose inclusion of an intermediate category between HIH and HA which may warrant closer follow-up.

1173 Is Mast Cell Infiltration Associated with a Reduced Response to Proton Pump Inhibitors in Pediatric Eosinophilic Esophagitis?

Paroma Bose[1], Katrina Collins[1], Christopher Miller[1], Djamilatou Adom[1], Pegah Mehrpouya_Bahrami[1], Anthony Perkins[1], Sandeep Gupta[1], Emily Hon[1], Mark Kaplan[1]
[1]Indiana University School of Medicine, Indianapolis, IN

Disclosures: Paroma Bose: None; Katrina Collins: None; Christopher Miller: None; Djamilatou Adom: None; Pegah Mehrpouya_Bahrami: None; Anthony Perkins: None; Sandeep Gupta: *Consultant*, Adare, Allakos, Regeneron, Celgene, Viaskin; Emily Hon: *Employee*, Eli Lilly and Co.; Mark Kaplan: None

Background: The variability of response to proton pump inhibitor (PPI) therapy in eosinophilic esophagitis (EoE) is poorly understood. It is well known that intraepithelial mast cell numbers are increased in EoE; however the role of mast cells and associated epithelial changes as a predictor of treatment response in EoE has yet to be established. We examined mast cell burden in esophageal biopsies of pediatric subjects with PPI-responsive (PPI-R) EoE, PPI-nonresponsive (PPI-NR) EoE, and non-EoE esophageal dysfunction (controls).

Design: Subjects undergoing diagnostic endoscopy for esophageal dysfunction were enrolled. Subjects with EoE, defined as ≥ 15 eosinophils/high powered field (hpf) on esophageal biopsy, were treated with 8 weeks of PPI therapy followed by repeat endoscopy. Subjects with < 15 eosinophils/hpf were defined as PPI-R EoE and ≥ 15 eosinophils/hpf as PPI-NR EoE. Total mast cells were quantified in esophageal biopsies using immunohistochemistry with CD117 (mean count/10 hpf) and were correlated with gene expression profiles using the Nanostring nCounter® Analysis System or RT-qPCR in subject samples from PPI-R EoE, PPI-NR EoE, and controls.

Results: Of 72 subjects enrolled, 41 met criteria for EoE and 25 had follow-up endoscopy after PPI therapy. Eight had PPI-R EoE and 17 had PPI-NR EoE. CD117 counts were significantly higher in EoE compared to controls [6.5±6.4 vs 1.1±2.5 (p<0.001)] but did not differ between PPI-R and PPI-NR EoE at baseline [3.0±2.4 vs 4.7±4.5 (p=0.535)]. Tryptase-beta-2 (TPSB2) and carboxypeptidase-3 (CPA3), enzymes involved in mast cell activation, were differentially expressed among PPI-R EoE, PPI-NR EoE, and controls at baseline. TPSB2 and CPA3 median gene expression was highest in PPI-NR EoE followed by PPI-R EoE and controls [H(3)=18.17, p=0.0001 and H(3)=13.06, p=0.0015 respectively]. See Figure for Kruskal Wallis ranks plots.

Figure 1 - 1173

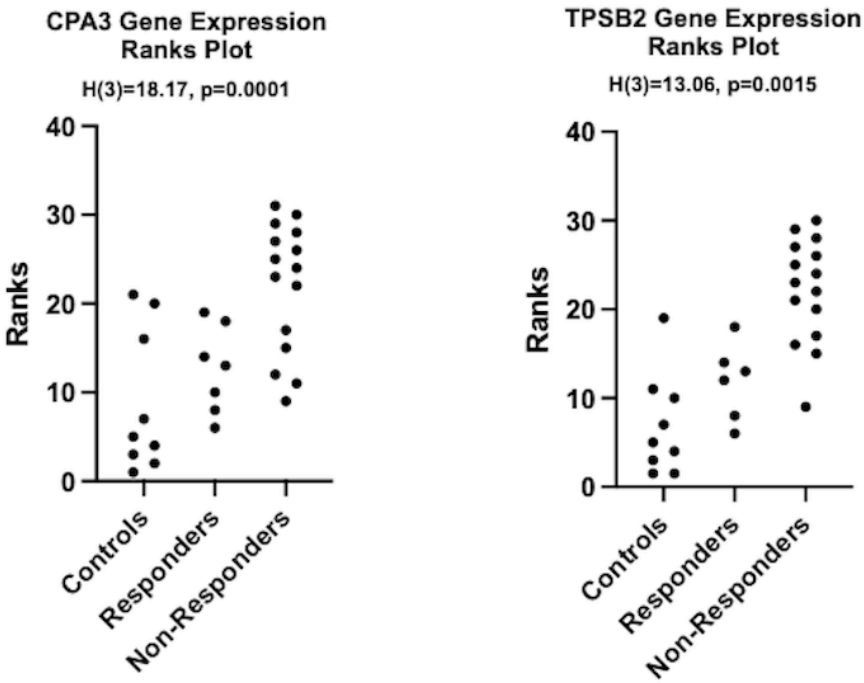

Conclusions: Although CD117 counts did not differ between PPI-R and PPI-NR EoE at baseline, subjects with PPI-NR EoE had higher expression of TPSB2 and CPA3 genes compared to PPI-R EoE. Mast cell activation may help identify PPI-R and PPI-NR EoE prior to treatment. Additional research is warranted to assess the role of mast cell activation on PPI effectiveness in EoE.

1174 Prenatal Stress Increases Frequency and Malignancy of Neuroblastoma Tumors in TH-MYCN Animal Model

Susana Galli[1], Sung-Hyeok Hong[1], Larissa Wietlisbach[1], Akanksha Mahajan[1], Jason Tilan[1], Joanna Kitlinska[1]
[1]Georgetown University Medical Center, Washington, DC

Disclosures: Susana Galli: None; Sung-Hyeok Hong: None; Larissa Wietlisbach: None; Akanksha Mahajan: None; Jason Tilan: None; Joanna Kitlinska: None

Background: Neuroblastoma (NB) is a pediatric malignancy arising due to defects in sympathetic neuron differentiation. NB is a heterogeneous disease, with phenotypes ranging from spontaneously regressing to highly aggressive, incurable tumors. This clinical variability cannot be explained solely by genetic aberrations. Even in families with hereditary NB the penetrance of the disease is incomplete and the same genetic mutation often results in tumors with phenotypes varying from differentiating ganglioneuromas to undifferentiated, highly aggressive NBs. Thus, other, perhaps non-genetic factors can contribute to the disease development and modify its phenotype. Strikingly, the two factors promoting de-differentiation of NB cells and their malignant phenotype, hypoxia and glucocorticoids, are elevated in the fetus during maternal stress, suggesting a role for prenatal stress in NB tumorigenesis.

Design: The goal of the current study was to determine the effect of prenatal stress on NB risk. To this end, pregnant mice carrying TH-MYCN hemizygous offspring were subjected to chronic unpredictable stress at embryonic days 10-17, the time of sympathetic neuroblast proliferation and differentiation. The tumor frequencies and metastasis were compared between offspring of control and stressed mothers.

Results: The offspring from the prenatally stressed group presented with increased tumor frequencies and more malignant disease, as manifested by the presence of advanced lung metastases disseminating from small primary tumors (<200 mm^3). This phenotype was associated with increased mortality in prenatally-stressed TH-MYCN offspring ($p<0.01$). In contrast, no advanced lung metastases and no disease-related deaths were observed in TH-MYCN offspring of control mothers despite the presence of large primary tumors (>500 mm^3). Although not common, lung metastases occur preferentially in NB patients with MYCN amplification and are associated with significantly worse prognosis, as compared to patients with metastatic disease, but no pulmonary involvement (14 vs 43% 3-year event-free survival, respectively). Thus, the profound pulmonary dissemination observed in prenatally-stressed TH-MYCN mice mimics one of the most malignant NB phenotypes observed in human disease.

Conclusions: Altogether, our data implicate maternal stress during pregnancy as a potential environmental factor modifying the effects of genetic aberrations and promoting development of NB with malignant phenotype.

1175 Identification of a Novel Long Spliced Internal Tandem Duplication of BCOR Exon 15 in Pediatric BCOR-Associated Sarcomas

Jian Yuan Goh[1], Kuick Hong[1], Jet Aw[2], Kenneth Chang[3]
[1]KK Women's and Children's Hospital, Singapore, Singapore, [2]Singhealth, Singapore, Singapore, [3]KKH, Singapore, Singapore

Disclosures: Jian Yuan Goh: None; Kuick Hong: None; Jet Aw: None; Kenneth Chang: None

Background: Clear cell sarcoma of the kidney (CCSK) and primitive myxoid mesenchymal tumor of infancy (PMMTI) are pediatric *BCOR*-associated sarcomas that most commonly harbor internal tandem duplications (ITD) of exon 15 of the *BCOR* gene. Some cases have alternative mutations viz. *BCOR-CCNB3* and *YWHAE-NUTM2* gene fusions. However, a small number of cases have none of the above mutations. As diagnosis of CCSK and PMMTI may be challenging by morphology and immunohistochemistry alone, it is important to identify a specific entity-defining mutation in such cases.

Design: We encountered two CCSKs and one PMMTI which did not have *BCOR* ITD or *BCOR-CCNB3* or *YWHAE-NUTM2* gene fusions detectable by standard testing methods. We therefore set out to identify the underlying mutation using an RNA-based next-generation sequencing anchored multiplex PCR (Archer FusionPlex) technique.

Results: By performing Archer FusionPlex using extracted RNA as input material, we identified two related *BCOR* exon 15 RNA transcripts with internal tandemly duplicated segments (hereafter 'ITD') that were 388 base pairs (bp) and 96 bp in length. At genomic DNA level, DNA sequencing identified only the 388 bp ITD which incorporated a stop codon and a 3' untranslated region. In silico analysis of this 388 bp ITD revealed acceptor and donor splice sites, indicating that at RNA level, the 388 bp ITD (representing precursor mRNA) is spliced to form the 96 bp ITD (representing mature mRNA). This novel and unusually long 388 bp ITD is difficult to identify by DNA sequencing using typical primer design strategies targeting entire duplicated segments, because a segment length of 388 bp is beyond typical read lengths of most sequencing platforms and usual fragment lengths of formalin-fixed and paraffin-embedded material. To confirm these findings, we performed Sanger sequencing using primers targeting the ITD breakpoint instead of the more conventional strategy targeting an entire duplicated segment.

Conclusions: We identify a novel *BCOR* exon 15 ITD that is 388 bp long; this 388 bp ITD is far longer than typical ITD lengths described to date of 87 to 114 bp. Following transcription, this novel ITD undergoes splicing in which the precursor mRNA bearing the 388 bp ITD is processed to generate a mature mRNA transcript bearing a shorter 96 bp ITD. Knowledge of this novel *BCOR* ITD is important in relation to primer design for detection by sequencing, and choice of starting material viz. RNA versus DNA for sequencing.

1176 Clinicopathologic Characteristics of Renal Cell Carcinomas in Pediatric Patients. A Pediatric Single Center Experience

Nilda Gonzalez Roibon[1], Maria Laura Galluzzo Mutti[1], Guido Felizzia[1], Dora Diaz[2], Maria Teresa de Davila[3], Jessica López Marti[1], Fabiana Lubieniecki[4]
[1]Hospital Garrahan, Buenos Aires, Argentina, [2]National Hospital of Pediatrics Dr. JP Garrahan, Buenos Aires, Argentina, [3]Pediatric Garrahan Hospital, Ciudad de Buenos Aires, Argentina, [4]Hospital de Pediatria J.P.Garrahan, Buenos Aires, Argentina

Disclosures: Nilda Gonzalez Roibon: None; Maria Laura Galluzzo Mutti: None; Guido Felizzia: None; Dora Diaz: None; Maria Teresa de Davila: None; Jessica López Marti: None; Fabiana Lubieniecki: None

Background: Renal cell carcinoma (RCC) is rare in pediatric age, accounting for less than 5% of renal tumors in this age group. Literature regarding incidence and clinicopathologic characteristics is scarce. The objective of this study was to describe clinicopathologic characteristics of RCC in children and adolescents in a single pediatric hospital, emphasizing the most frequently identified subtypes.

Design: We queried our surgical pathology files for cases with the diagnosis of RCC between 2001 and 2019. Whole sections from formalin-fixed paraffin-embedded tissue were assessed for confirmation of diagnosis. Appropriate immunohistochemistry (IHC) and Fluorescence in situ hybridization (FISH) for TFE3 rearrangement were performed. Diagnosis was made following WHO 2016 classification and staging was assigned following AJCC 8th Ed.

Results: We identified 21 cases of carcinomas and 1 oncocytoma. Median age at diagnosis was 12 years (3-17); 16 patients (73%) were female. Left sided tumors were slightly more frequent (7/13) and none were bilateral. Complete clinical information was available in 9 cases. One patient had history of chemotherapy for bilateral retinoblastoma. Most patients (5/9) presented with disseminated disease at diagnosis (distant lymph nodes, central nervous system and bone metastasis). Two patients had advanced local disease with unresectable tumors. Median follow up was 33 months (3-149 months). Five patients were on palliative care at last follow up. MiT family translocation RCC was the most common variant in this age group (13/21), based on FISH positivity for TFE3 rearrangement. PCR was performed in 10 of these cases and was assessable in 4 (ASPLex7-TFE3ex6 in 2 cases, and TFE3ex3-PRCCex2 and PSFex9-TFE3ex5, 1 case each; 5 transcripts studied were not detected in 1 case). Other variants identified were papillary, chromophobe and ALK translocation associated carcinoma (both FISH and PCR positive), 1 case each. One case remained unclassifiable, one case showed histology suggestive of HLR- associated RCC and another case suggestive of TFEB translocation carcinoma.

Conclusions: Our results suggest that the most frequent variant of RCC in children is MiT family translocation and that these cases are aggressive with advanced stage at diagnosis. It is noteworthy that most of the knowledge regarding RCC in children is based on tumors occurring in adults, specially clear cell RCC. Further studies may be necessary to establish the optimal diagnostic and therapeutic regimen.

1177 Single Institutional Experience with Defining Ewing, Ewing-Like, and Undifferentiated Sarcoma Cases Over the Previous Decade

Jessica Gulliver[1], Melissa Mejia Bautista[2], Kai Lee Yap[1], Pauline Chou[3]
[1]Ann & Robert H. Lurie Children's Hospital of Chicago, Chicago, IL, [2]McGaw Medical Center of Northwestern University, Chicago, IL, [3]Lurie Children's Hospital of Chicago, Chicago, IL

Disclosures: Jessica Gulliver: None; Melissa Mejia Bautista: None; Kai Lee Yap: None; Pauline Chou: None

Background: Ewing or Ewing-like sarcoma and undifferentiated small round cell sarcomas represent an ever changing group of tumors. As more molecular testing platforms become available, additional fusions and pathognomonic mutations have been identified. This series evaluates a single institution's experience with suspected Ewing, Ewing-like and undifferentiated sarcomas over the past decade.

Design: Non-hematopoietic round cell sarcoma cases were collected from 2010-2020. Based on their morphologic and immunohistochemical profile, the tumors were initially classified as Ewing, Ewing-like or undifferentiated sarcoma. Next generation sequencing became available in 2019 at our institution and many of these tumors were reanalyzed for the types of fusions, frequency of fusions. While most tumors have available tissue for reclassification, others do not lend additional material for the study.

Results: A total of 57 sarcomas were analyzed. The patients ranged from 2-31 years of age. 44 were male and 13 were female. 31 were positive for EWSR1-FLI1 rearrangement, 3 were positive for EWSR1-ERG rearrangement and 2 were positive for a FUS-ERG rearrangement confirming the original diagnosis of Ewing sarcoma. While others diagnosed originally as either Ewing-like or Undifferentiated were found to have the following: BCOR rearrangement (x2), CIC-DUX4 (x1) rearrangement, EWSR1-CREB rearrangement (x1) and 9 had no identifiable fusion by RT-PCR, but 2 subsequently were found to have EWSR1-POU5F. 5 were positive for EWSR1 rearrangement by FISH but without additional details. In addition to EWSR1-FLI1 rearrangement, one of the cases also had a mutation involving the TERT promoter. One case with EWSR1-ERG rearrangement had an additional mutation in TP53. One case with an FUS-ERG rearrangement had a mutation involving NF1.

Conclusions: Small round cell sarcomas are diagnostically challenging but increasingly are now better defined by their molecular abnormalities. In this case series, EWSR1-FLI1 continued to represent the most common EWSR1 rearrangement. However, unique rearrangements involving POU5F, CREB, FUS-ERG, BCOR, and CIC-DUX4 were also identified. Unique rearrangements involving EWSR1 should be considered when performing molecular studies. The detection of alternate rearrangements is important because it may change the diagnosis from Ewing sarcoma to other types of sarcoma as occurred in this case series.

1178 SARS-CoV-2 Placentitis with Intraparenchymal Thrombohematomas: Association with Intrauterine Fetal Demise, Perinatal Morbidity, and Ultrasonographic Findings

Anh Huynh[1], Ilona Goldfarb[1], Jaclyn Watkins[2], Vanda Torous[1], Jennifer Sehn[3], Drucilla Roberts[1]
[1]Massachusetts General Hospital, Boston, MA, [2]Massachusetts General Hospital, Harvard Medical School, Boston, MA, [3]St. Louis University School of Medicine, St. Louis, MO

Disclosures: Anh Huynh: None; Ilona Goldfarb: None; Jaclyn Watkins: None; Vanda Torous: None; Jennifer Sehn: None; Drucilla Roberts: None

Background: SARS-CoV-2 placentitis is defined by the triad of histiocytic or mixed inflammatory intervillositis, increased perivillous fibrin deposition, and villous trophoblastic necrosis. We have observed multiple cases of intrauterine fetal demise (IUFD) or perinatal morbidity with intraparenchymal thrombohematomas, a feature not previously linked to poor outcomes associated with SARS-CoV-2-placentitis. Here we present 17 cases with such findings and provide a possible point of intervention as these lesions can be identified by ultrasonography.

Design: A retrospective study, approved by the Institutional Review Board, was performed by searching the terms “SARS-CoV-2 placentitis” or “SARS-CoV-2 infection” or “COVID” in our pathology database for all in-house deliveries and cases from the consult practice of the authors between 1/1/21 and 9/24/21. Clinical data was obtained via the electronic medical records or through contacting the consulting pathologists.

Results: Twenty-three cases were retrieved and reviewed for the presence of thrombohematomas in the maternal space. Seventeen cases had thrombohematomas, intervillous thrombi, or intervillous hemorrhage in addition to classic SARS-CoV-2 placentitis, and 12 of those cases (71%) were associated with IUFD. The period between a positive maternal COVID test and loss was less than 14 days in all but three cases of IUFD (75%). The non-IUFD cases were all associated with other perinatal morbidity. In 8 of 17 cases (47%), thrombohematomas were noted grossly. The presence of “multiple placental lakes” were identified in three cases where placental imaging was available. Representative gross and histologic findings and an ultrasound displaying “placental lakes” are presented in Figures 1 and 2, respectively. Clinical data associated with each case is in Table 1.

Table 1. Clinical findings of cases with thrombohematomas. MA indicates maternal age; G, gravida; P, para; IUFD, intrauterine fetal demise; LB, live birth; GA, gestational age; NA, not applicable/unknown; GDM, gestational diabetes; NRFHT, non-reassuring fetal heart tracing; BPP, biophysical profile; IUGR, intrauterine growth restriction.

Case	MA	G	P	IUFD or LB	GA at loss or delivery (weeks + days)	Days from COVID-19 positive test to loss or delivery	Maternal COVID-19 symptoms peripartum	Pregnancy complications & comorbidities	Apgar Score at 1, 5, and 10	Neonatal course
1	39	4	2 - > 3	IUFD	26+2	2	Disseminated intravascular coagulation (DIC)	NA		
2	37	5	2 - >3	IUFD	30+4	3	Fever, cough, loss of taste, diarrhea, fatigue	atypical HELLP (thrombocytopenia, elevated liver enzymes, low fibrinogen)		
3	39	6	5 - > 6	IUFD	37+1	10	Body aches, fever	NA		
4	37	4	2 - > 3	IUFD	33+0	5	Body aches, fever	Third trimester GDM		
5	31	1	0 - > 1	IUFD	32+5	NA	Cough, shortness of breath, severe body aches, fatigue, loss of taste and smell, and diarrhea	Thrombocytopenia, elevated liver enzymes, low fibrinogen		
6	NA	NA	NA	IUFD	NA	NA	NA	NA		
7	28	NA	NA	IUFD	31+3	13	NA	NA		
8	22	1	0 - > 1	IUFD	25+0	NA	NA	Maternal history of gonorrhea		
9	26	2	0 - > 1	IUFD	27+1	7	NA	Pre-eclampsia with severe features		
10	24	2	1 - > 2	IUFD	32+6	17	Asymptomatic	NA		
11	37	4	2 - > 3	IUFD	27+3	2	Asymptomatic	Presented with decreased fetal movement		
12	41	NA	NA	IUFD	NA	8	NA	NA		
13	32	2	0 - > 1	LB	32+0	6	Pneumonia requiring intubation	Third trimester maternal anemia	1, 4, 6	Complications of prematurity, required intubation
14	30	NA	NA	LB	38+5	14	Body aches and chills	Fetal intolerance to labor and thick meconium at delivery	2, 4, 7	NA
15	28	NA	NA	LB	32+0	12	Asymptomatic	NRFHT and BPP 0/10 prompting emergent delivery	NA	NA
16	26	1	0 - > 1	LB	28+6	11	Pneumonia requiring intubation, hypotension	Abnormal fibrinogen, transaminitis but and no other symptoms of pre-eclampsia; oligohydramnios	1, 6, 7	Complications of prematurity
17	30	NA	NA	LB	31+0	21	Pneumonia	IUGR, congenital anomalies	NA	NA

Figure 1 - 1178

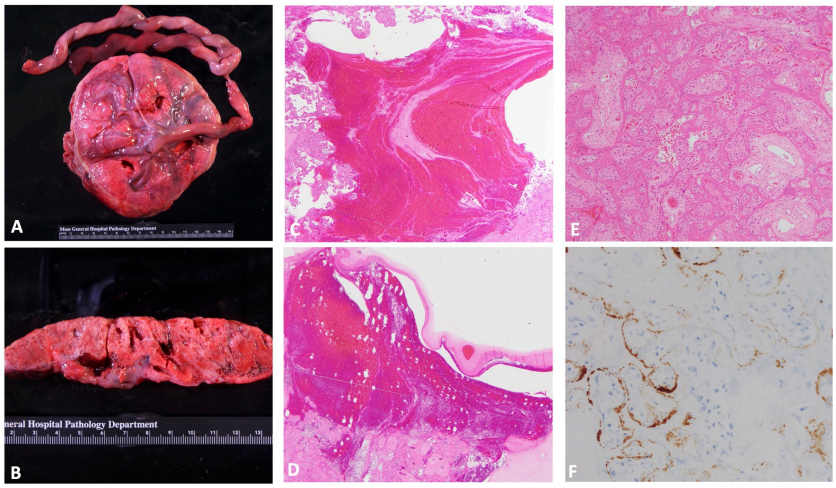

Figure 1. Gross and histologic findings of thrombohematomas in a SARS-CoV-2-positive placenta. A-B) Gross photographs with blood-filled spaces. C-D) H&E sections with thrombohematomas. E) H&E section with background SARS-CoV-2 placentitis. F) Positive SARS-CoV-2 RNA-ISH.

Figure 2 - 1178

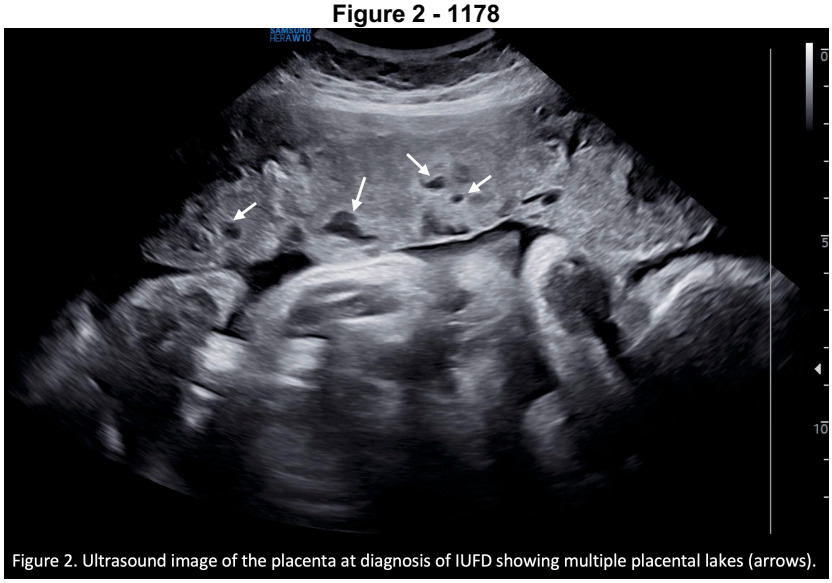

Figure 2. Ultrasound image of the placenta at diagnosis of IUFD showing multiple placental lakes (arrows).

Conclusions: We identify a novel feature present in placentas with SARS-CoV-2 placentitis associated with poor outcomes. The often grossly identifiable thrombohematomas were present in 17 cases of SARS-CoV-2 placentitis, the majority of which were associated with IUFD, suggesting that their presence is a marker for increased perinatal morbidity and mortality. We also show that these thrombohematomas can be identified by ultrasound, demonstrating that imaging the placenta is critical in pregnancies affected by COVID-19 independent of maternal symptoms as it may identify markers of severe placental damage that can be associated with IUFD or significant perinatal morbidity.

1179 Paratesticular Extramedullary Hematopoiesis in Children

Elisabetta Kuhn[1], Letterio Runza[2], Umberto Gianelli[3]
[1]Fondazione IRCCS Ca' Granda Ospedale Maggiore Policlinico, University of Milan, Italy, [2]Fondazione IRCCS Ca' Granda Ospedale Maggiore Policlinico, Milan, Italy, [3]IRCCS Ca' Granda - Maggiore Policlinico Hospital Foundation, Milan, Italy

Disclosures: Elisabetta Kuhn: None; Letterio Runza: None; Umberto Gianelli: None

Background: Extramedullary hematopoiesis (EMH) is an uncommon occurrence in routine pathology practice. Although usually it is associated with hematologic disorders, sporadically it is an isolated finding, particularly in children. This study aims to determine

the frequency, immunomorphological characteristics, and clinicopathological background of EMH in orchiectomies from pediatric patients.

Design: All orchiectomy specimens from pediatric patients (<18 years of age) removed from 2008 to 2020 in our institution were retrieved and reviewed retrospectively. Testicular biopsies and neoplasias were not included. The diagnosis of EMH was given when immature hematopoietic cell clusters were present. Immunohistochemical stainings for glycophorin A, E-cadherin, myeloperoxidase, CD43, TdT, CD68, CD45, CD34, CD117, CD61, and ki-67 were performed. EMH foci were classified according to the amount of EMH, their hematopoietic components (erythroid, myeloid, or trilineage), side, and pathological background.

Results: 78 orchiectomies were performed in pediatric patients (mean age 5 years, range 0 years to 17 years) at our institution for benign pathologies. Among them 40 testicles (52.5%) were removed for testicular atrophy, 34 (43.6%) for testicular torsion and, 3 (3.9%) showed disorders of sexual differentiation. EMH was identified in 6 of 78 orchiectomies (7.7%), all operated for testicular torsion. All but one patient were newborns and, the remaining patient was 15 years old. In no case there was evidence of hematologic disorder. In all cases EMH was an incidental and microscopic finding, with variable extension, from a few clusters of about 50 cells to many clusters of hundreds of cells. Immunohistochemical stainings confirmed an association of myeloid (myeloperoxidase+) and erythroid precursors (glycophorin A+/E-cadherin+) in all 6 cases. Among them, one case presented also rare megakaryocytes (CD61+), and one case intermingled benign lymphocytic precursors (TdT+). In 4 cases EMH foci were in the connective tissue of the epididymis, often with perivascular cuffing distribution, and in 2 cases in the stroma of the ductus deferens. All EMH foci were in a background of granulation tissue, containing extravasated erythrocytes and hemosiderin deposition.

Conclusions: To our knowledge, this is the first study that demonstrates EMH as a common, incidental finding in orchiectomy samples, especially from newborns. Despite the lack of pathological potential, it is important to recognize EMH in order to avoid misdiagnosis.

1180 Methylomic Profiling of Pediatric Primary Malignant Neurocutaneous Melanocytic Neoplasm Involving Central Nervous System

Aofei Li[1], Claudia Salgado[2], Dipanjan Basu[3], Yasmin Khakoo[4], Bruce Bauer[5], Fangping Mu[6], Uma Chandran[7], Miguel Reyes-Múgica[8]

[1]University of Pittsburgh, UPMC, Pittsburgh, PA, [2]Children's Hospital of Pittsburgh, Pittsburgh, PA, [3]University of Pittsburgh School of Medicine, Pittsburgh, PA, [4]Memorial Sloan Kettering Cancer Center/Weill Cornell Medical College, New York, NY, [5]University of Chicago, Chicago, IL, [6]University of Pittsburgh, Pittsburgh, PA, [7]University of Pittsburgh Medical Center, Pittsburgh, PA, [8]UPMC Children's Hospital of Pittsburgh, Pittsburgh, PA

Disclosures: Aofei Li: None; Claudia Salgado: None; Dipanjan Basu: None; Yasmin Khakoo: None; Bruce Bauer: None; Fangping Mu: None; Uma Chandran: None; Miguel Reyes-Múgica: None

Background: Large/Giant congenital melanocytic nevi (L/GCMN) are rare congenital lesions mostly caused by NRAS or BRAF mutations. There is a » 4% lifetime risk of malignant transformation into primary malignant neurocutaneous melanocytic neoplasm (PMNMN) which frequently involves the central nervous system (CNS). The pathogenesis and diagnostic criteria of PMNMN differ from adult cutaneous melanoma and are poorly understood. DNA methylation is an epigenetic mechanism involved in the oncogenesis of many cancer types. Methylomics has emerged as an important diagnostic tool in CNS tumors. However, the methylome of PMNMN is not well studied. We hereby report the largest-to-date genome-wide methylomic profiling of PMNMN.

Design: 167 L/GCMN cases were selected from the Gavin Bailey Tissue Repository for Neural Crest Disorders, of which 8 cases developed PMNMN. Histology, immunohistochemistry and next-generation sequencing findings were reviewed for establishing diagnosis. Methylomic profiling was performed on L/GCMN and PMNMN with Illumina MethylationEPIC BeadChip Kit. The methylome data were analyzed with Illumina Genome Studio, Partek Genomics Suite and DKFZ CNS methylation classifier.

Results: The 8 patients with CNS PMNMN ranged from 1.5 to 12 years old, with equal gender distribution. All patients succumbed to the disease, with 2 cases showing peritoneal metastasis via VP-shunts. All tumors had activating NRAS mutations, with variable additional genetic alterations involving KIT, P53, MYC, MLH1 and NF1. By DKFZ methylation database, 4 tumors were classified as melanocytoma (calibrated score 0.42 - 0.65), 1 as meningioma, 1 as CIC-altered Ewing sarcoma and 2 as non-contributory. In comparison to the paired L/GCMN, PMNMN showed significant copy number variations by Illumina BeadChip and frequently had 8p locus (FGFR1, MYC) amplification. Differential methylation analysis of CNS PMNMN in reference to L/GCMN revealed significant promoter hypermethylation in a number of gene loci including tumor suppressors (e.g. CDH1 and RAD50), as well as promoter hypomethylation in gene loci including oncogenes (e.g. TCF4).

Conclusions: We report the largest-to-date genome-wide methylomic profiling of PMNMN, highlighting genetic alterations distinct from metastatic cutaneous melanoma and other primary CNS melanomas. We show genetic and epigenetic alterations possibly driving the progression from L/GCMN to PMNMN. These findings provide information on the molecular diagnosis and pathogenesis of PMNMN.

1181 Histologic Findings in Large for Gestational Age Placentas and Correlation with CD15, A Potential Marker of Pathological Villous Immaturity

Ansa Mehreen[1], Linda Ernst[2]
[1]University of Chicago NorthShore, Evanston, IL, [2]University of Chicago at NorthShore HealthSystem, Evanston, IL

Disclosures: Ansa Mehreen: None; Linda Ernst: None

Background: Large for gestational age (LGA) placentas weigh > 90th percentile for the gestational age and may show delayed villous maturation (DVM) on histology. CD15 has recently been reported to show increased expression in the endothelium of fetoplacental vessels of immature villi. In this study, we aim to examine the percentage of CD15 staining in the villous vasculature of LGA placentas vs appropriate for gestational age (AGA) placentas and document the other potential histologic findings in LGA placentas.

Design: For this case control study, LGA placentas (>90th percentile) and AGA placentas from term pregnancies (37-41 weeks) were selected from our pathology database between 01/2018- 06/2021. We extracted demographic and pathologic findings from pathology reports. Major pathologic findings included: acute inflammation (AI), chronic inflammation (CI), maternal vascular malperfusion (MVM), fetal vascular malperfusion (FVM), DVM and villous hypervascularity/chorangiosis. A representative block of placental parenchyma was selected for CD15 immunohistochemistry. Stained slides were reviewed in a random order, blinded to the placental weight. Five random 20x fields were scored semi-quantitatively for CD15 staining of villous capillaries on a scale of 0-5 (0=0%, 1=1-5%, 2=5-25%, 3=25-50%, 4=50-75%, 5=>75%). Statistical analysis was performed using IBM SPSS Statistic 22.

Results: 75 LGA placentas and 73 AGA controls were analyzed. The average score of CD15 staining in villous capillaries was significantly higher amongst the LGA placentas (Figure 1). The average placental weight and birth weight was also significantly higher in the LGA group than the AGA. AI, CI, FVM, DVM and villous hypervascularity/chorangiosis were all significantly more prevalent in LGA placentas than in AGA placentas. No significant differences were seen in the prevalence of Gestational diabetes mellitus (GDM), hypertension (HTN) or preeclampsia between AGA and LGA placentas (Table 1).

Table 1

Demographic data	LGA placentas (N=75)	AGA placentas (N=73)	p-value
Placental weight (g)	755 ± 62	487 ± 41	<0.001
Birth weight (g)	4128 ± 486	3356 ± 369	<0.001
Maternal age (yrs)	32.9 ± 4.8	32.6 ± 4.9	NS
Gestational age (wks)	38.7 ± 1.12	38.4 ± 0.97	NS
Placental histologic findings			
CD15 score (average of 5 20x fields)	2.7 ± 1.1	1.8 ± 0.87	<0.001
MVM	9%	2.7%	NS
FVM	27%	2.7%	0.000
AI	77%	30%	0.000
CI	33%	12%	0.003
DVM	23%	0%	0.000
Villous hypervascularity/ Chorangiosis	25%	6.8%	0.003
Maternal pregnancy complications			
GDM	32%	23%	NS
HTN	36%	34%	NS
Preeclampsia	11%	10%	NS

Figure 1 - 1181

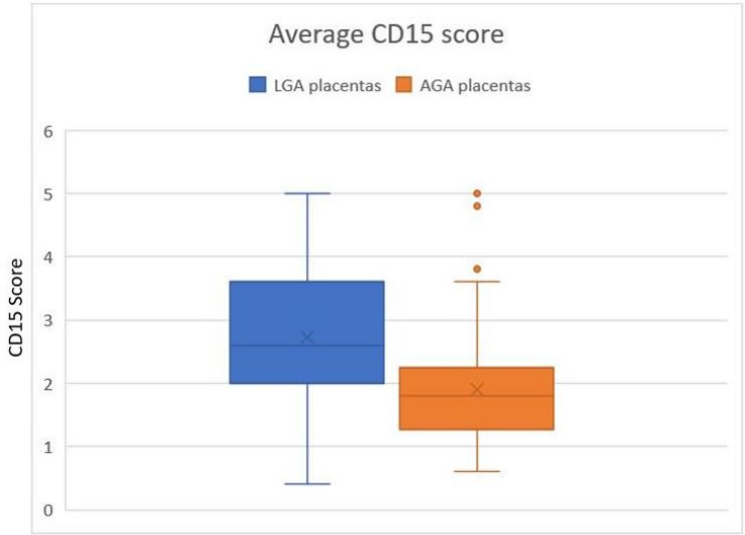

Conclusions: LGA placentas have increased expression of CD15 in villous capillary endothelium and higher prevalence of DVM. Our data suggests that CD15 stain can be used as an objective marker of villous immaturity. Also, another novel finding of our study is the higher prevalence of inflammation and FVM in LGA placentas potentially indicating an adverse intrauterine environment.

1182 Submucosal Nerve Trunk Diameter Associated With Rectal Suction Biopsy Is a Valuable Diagnostic Marker For Hirschprung's Disease

Lili Miles[1], Lisvet Luceno[2], Roberto Gomez-Suarez[1], Shannon Henry[1], Michael Miles[2]
[1]Nemours Children's Hospital, Orlando, FL, [2]University of Central Florida College of Medicine, Orlando, FL

Disclosures: Lili Miles: None; Lisvet Luceno: None; Roberto Gomez-Suarez: None; Shannon Henry: None; Michael Miles: None

Background: Aganglionosis is the gold standard diagnostic test for patients with suspected Hirshprung's disease (HD). The use of the morphometric analysis of submucosal nerve hypertrophy in aganglionic bowel of patients with HD has been debated. Rectal suction biopsy (RSB) is particularly valuable in newborns with delayed passage of meconium, and in older children with challenging constipation and absence of rectoanal inhibitory reflex. Nerve trunk diameter may be supportive for the diagnosis of HD, however, it has been questioned as a diagnostic criterion for HD due to possible age-related variation. The purpose of this study is to evaluate the diagnostic value of nerve hypertrophy in consecutive pediatric patients who had RSB to rule out HD.

Design: This retrospective study was approved by the institutional review board. Between Jan. 2013 and Sep. 2021 all patients who had RSB to rule-out HD were identified. Only patients with an adequate biopsy specimen were included. Nerve trunk diameter was measured by an experienced pediatric pathologist (LM) using a micrometer eyepiece. If one nerve trunk diameter ≥40 µm was observed, the two largest nerves were measured, and the average used in the data analysis. Data were stratified according to the positive diagnosis of HD, a history of chronic constipation (CC), and no history of CC (non-CC). Receiver operator characteristic (ROC) analysis was used to determine false positives, false negatives, and optimal cutoff value for nerve diameter.

Results: A total of 96 patients (48 females; 50%) were identified, including 11 (11.5%) with HD, 76 (79.2%) with a history of CC, and 9 (9.4%) non-CC. Most patients in the non-CC group (8/9; 89%) were younger than 3 months, and it was defined as a disease control group. Age at RSB was significantly increased in the CC group, but similar between the control and HD groups (Table). Average nerve trunk diameter was significantly increased in HD patients compared with control and CC groups (Table), but not significantly different between CC and non-CC groups. Nerve trunk diameter was not associated with age or history of CC. ROC analysis showed that nerve trunk diameter was 100% specific and sensitive for HD; that ROC AUC was 1.0; and that 43 µm was an optimal cutoff.

	Controls [Mean(SD)/Median]	CC Group [Mean(SD)/Median]	HD Group [Mean(SD)/Median]	P-value (Controls vs HD)	P-value (CC vs HD)	P-value (Non-HD vs HD)
N	9	76	11			
Age (mos)	1.8(2.7)/0.9	47.2(47.5)/35.2	11.9(20.4)/0.5	0.76	<.0001	0.001
Submucosal Depth Max[a] (µm)	992(695)/790	793(508)/700	855(486)/900	0.85	0.46	0.52
Nerve Trunk Diameter Avg[b] (µm)	23.1(6.9)/20.0	28.1(6.7)/27.5	65.4(18.6)/60.0	<.0001	<.0001	<.0001
Muscularis Mucosa Thickness Max[a] (µm)	232(404)/100	269(175)/238	139(99)/100	0.79	0.01	0.02
CC, Chronic Constipation; HD, Hirschprung's disease [a]Max, maximum measured single value; [b]Avg, average of 2 maximum values if one is ≥40 µm. Non-parametric comparison.						

Conclusions: The presence of at least two hypertrophic nerves (>43 µm in diameter) on RSB is highly specific and sensitive for HD. Data suggest that nerve trunk diameter is independent of age and history of CC. A larger study is needed to confirm these results.

1183 The Initial Pathological Diagnosis of Ganglioneuroblastoma, Intermixed, at Presentation: The Clinicopathological Implications

Behtash Nezami[1], Mohammed Alghamdi[1], Fiorella Cardenas[1], Judy Sarungbam[1], S. Joseph Sirintrapun[1], Anuradha Gopalan[1], Ying-Bei Chen[1], Hikmat Al-Ahmadie[1], Victor Reuter[1], Shakeel Modak[1], Satish Tickoo[1]
[1]Memorial Sloan Kettering Cancer Center, New York, NY

Disclosures: Behtash Nezami: None; Mohammed Alghamdi: None; Fiorella Cardenas: None; Judy Sarungbam: *Consultant*, Janssen Research & Development, LLC; S. Joseph Sirintrapun: None; Anuradha Gopalan: None; Ying-Bei Chen: None; Hikmat Al-Ahmadie: *Consultant*, AstraZeneca, Janssen Biotech, Paige.ai; Victor Reuter: None; Shakeel Modak: None; Satish Tickoo: None

Background: International Neuroblastoma Risk Group (INRG) consensus pretreatment classification schema stratifies patients into low, intermediate, and high-risk using the patient age, clinical stage, histology, 11q aberrations and amplification of *MYCN* gene. We studied patients with the primary pathologic diagnosis of Ganglioneuroblastoma Intermixed (GNBI) - regarded as a tumor with "favorable" histology by International Neuroblastoma Pathology Classification (INPC) system - to evaluate the correlation of this diagnosis with the clinicopathological features.

Design: Retrospective search of the archives of the pathology department of our institution between 1995 and 2021 revealed 68 patients with the primary diagnosis of GNBI at presentation. Clinical follow up data was available for 57 of these patients, *MYCN* amplification status for all patients, and targeted exome sequencing data for 22.

Results: Clinical stage was determined based on clinical/radiological (including MIBG scanning) data and pathological confirmation, revealing 15/57 patients (26%) with metastatic disease at presentation (12 bone marrow, 3 soft tissue; median age: 2.5 years), and 42 patients with locoregional disease (74%; median age 4.7 years). *MYCN* amplification was detected in 2 patients (3.5%), both in the metastatic group. Over a median follow up of 3.7 years (range 0.3-15.5), all patients with locoregional disease (n=42) remained free of disease, while 8/15 with metastatic GNBI (53%) relapsed (Figure. 1); 2 of the latter died of disease. Single gene (*ALK*, *BRIP1*, *MDM2*, *NUP93*, *RARA*, *MYCN*, or *ROS1*, in 7 patients) and 2 gene (*BRCA2* and *NOTCH1*, 1 patient) somatic alterations were detected overall in 8 patients. The differences between the presence of mutations combined with *MYCN* amplification were statistically significant between metastatic and locoregional patients (p = 0.003).

Figure 1 - 1183

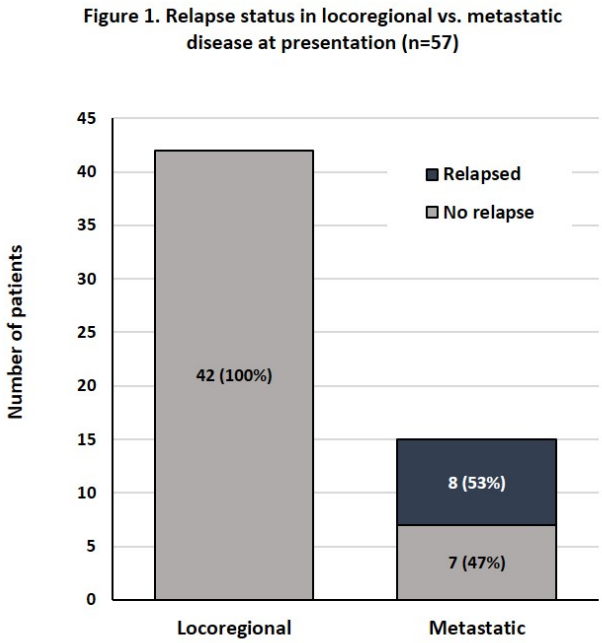

Conclusions: Localized GNBI at diagnosis has excellent long-term clinical outcome. However, a proportion of cases with this pathologic diagnosis have metastases at the time of initial diagnosis. Therefore, rendering "favorable" histology in pathology reports of primary GNBI in the absence of concurrent clinical and radiologic data may not reflect the true nature of disease in some cases. Very few patients with the initial diagnosis of GNBI show *MYCN* amplification.

1184 A Soft Tissue Tumor with EML4-ALK Fusion, Granular Cell Changes, Metastasis, and Response to Kinase Inhibitor Therapy in a Young Girl

Zhenhong Qu[1], Chris Hysell[1], Ping Zhang[2], Mark Micale[1]
[1]Beaumont Health, Royal Oak, MI, [2]William Beaumont Hospital, Birmingham, MI

Disclosures: Zhenhong Qu: None; Chris Hysell: None; Ping Zhang: None; Mark Micale: None

Background: An increasing number of soft tissue neoplasms with fusion of well-defined driver genes are being discovered. We report such a case in a 3-year-old girl with a 2-year follow-up.

Design: The patient first presented at age of 3.5 years with a painless right axillary/chest wall mass without constitutional symptoms. MRI demonstrated a 4.5 x 3.5 x 3.5 cm T2 hyper- and T1 hypointense mass. The mass was excised and showed a well-demarcated solid lesion with a homogeneous pale-white fleshy cut surface. No necrosis, myxoid or cystic change, hemorrhage, or calcification was noted. Microscopically, it was a variably hypercellular lesion composed of two main distinct cell types: oval fibroblast-like cells arranged in sheets with focal transition to spindle cells in whirling or storiform, and ganglion-like cells with abundant pale granular cytoplasm singly or in small clusters scattered among the fibroblast-like cells (Figure-1). Fibroblast-like cells contained a single resinoid nucleus with an irregular nuclear membrane surrounded by variable amount of eosinophilic cytoplasm with indistinct cell borders. Focal nuclear clustering and molding were seen. Patchy mild lymphocytic infiltrate was noted. No nuclear pleomorphism, necrosis or mitotic figure was identified. Immunohistochemically, both types of tumor cells were diffusely positive for ALK, CD34 and TFE3 (Figure-2) but negative for most lineage markers (Table). Next-generation-sequencing revealed EML4-ALK gene fusion of 5 a/b variant. No NTRK gene rearrangement was detected.

Results: The tumor recurred in 13 months with metastasis to regional lymph nodes and right lung. Biopsy showed similar morphology and immunohistochemical profile. Treatment with oral ALK inhibitor (crizotinib) was initiated at 200 mg BID. Seven weeks later, CT scan demonstrated partial radiological response with a measurable decrease in the main tumor size from 8.7 to 7.5 cm. The tumor regrew to 9.0 x 7.0 x 7.0 cm and became firm nine weeks thereafter crizotinib was inadvertently discontinued by her

mother. Reinstituting the therapy led to second tumor reduction (to 8.7 x 5.4 x 6.4 cm) and tumor softening on palpation. The patient is currently alive, active, and stable without any constitutional symptoms.

Table. Immunohistochemical Stain Result

Positive Stains	Focally Positive	Negative Stains
ALK (D5F3) CD34 TFE3 INI-1 (retained) SMARCA4 (retained) SMARCB1 (retained)	CD68 MITF SMA PU.1	AE13, calretinin, CAMTA-1 CD1a, CD19, CD21, CD23, CD31, CD117, CD163, chromogranin, Desmin, DOG1, EMA, ERG, GFAP, HMB45, MART1, MUC4, MSA, Myogenin, NUT1, P40, SOX10, S100, STAT6, synaptophysin

Figure 1 - 1184

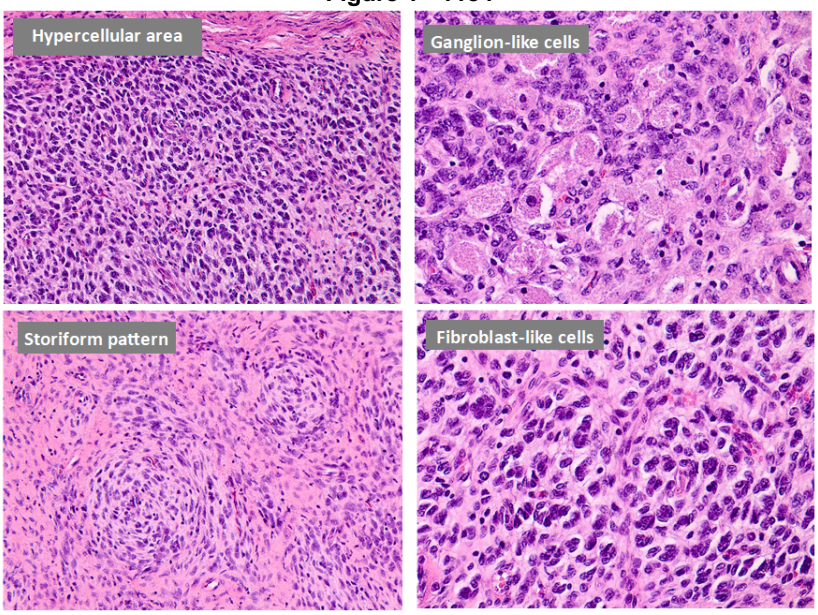

Figure 2 - 1184

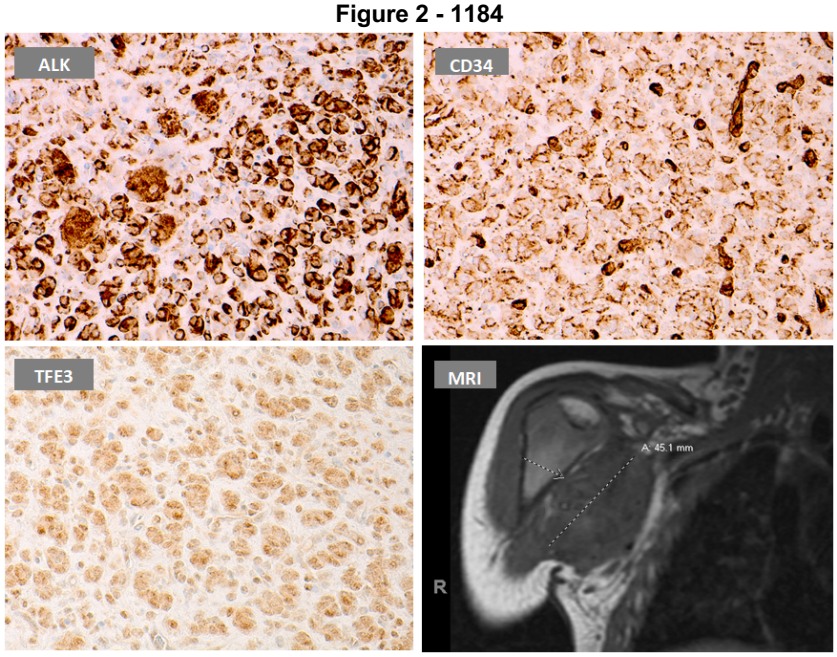

Conclusions: This tumor's features of EML4-ALK gene fusion, distinct innocuous histology, but rapid growth and metastasis, and response to ALK inhibitor add to the pathological and clinical spectrum of the kinase fusion-positive soft tissue neoplasms.

1185 Characteristic Histological and Molecular Findings in SARS-CoV-2-infected Placentas and its Impact on the Fetus. Study of 279 Cases from Pregnant Women Affected by COVID-19 during the Pandemic

Lourdes Salazar Huayna[1], Alexandra Navarro Jimenez[2], Jessica Camacho, Alfons Nadal[3], Joan Carles Ferreres[4], Javier Hernandez-Losa[5], Marta Sesé[6], Teresa Moline[7], Lourdes Naranjo[8], Louis Moscoso[1], Santiago Ramon Y Cajal[9], Marta Garrido-Pontnou[1]

[1]Hospital Universitari Vall d'Hebron, Barcelona, Spain, [2]Hospital Vall d'Hebron, Barcelona, Spain, [3]Hospital Clinic, Barcelona, Spain, [4]Hospital Parc Tauli, Barcelona, Spain, [5]Hospital Universitari Vall d'Hebron, VHIR, CIBERONC, Barcelona, Spain, [6]Molecular Pathology Group, Vall d´Hebron Institute Research, Barcelona, Spain, [7]Vall d'Hebron Research Institute, Barcelona, Spain, [8]University Hospital Vall d' Hebron, Barcelona, Spain, [9]Vall d'Hebron University Hospital, Barcelona, Spain

Disclosures: Lourdes Salazar Huayna: None; Alexandra Navarro Jimenez: None; Jessica Camacho: None; Alfons Nadal: None; Joan Carles Ferreres: None; Javier Hernandez-Losa: None; Marta Sesé: None; Teresa Moline: None; Lourdes Naranjo: None; Louis Moscoso: None; Santiago Ramon Y Cajal: None; Marta Garrido-Pontnou: None

Background: Placental pathology in pregnant women infected by SARS-CoV-2 has generated many reports with non-specific or contradictory results. The objective is to identify histological and molecular findings of infected placentas and its impact on the course of pregnancy.

Design: Placentas from 279 women infected with SARS-CoV-2 during pregnancy were reviewed, 137 of them with active infection within 10 days prior to delivery and 142 with past infection beyond this period. Four fetal autopsies were submitted for pathological study. Placental and fetal infection was investigated by immunohistochemistry (IHC) in 279 cases, RT-PCR in 27 cases and in situ hybridization (ISH) in 5 cases. Significance of association between qualitative variables was tested by Fisher's exact test.

Results: SARS-CoV-2 infection of placental tissues was demonstrated in 16/279 (5,7%) by IHQ (granular cytoplasmic villous trophoblast staining) and confirmed by ISH and RT-PCR (carried on 5 IHQ positive cases). All these 16 infected placentas showed diffuse (6/16) or focal (10/16) Trophoblast Damage (DTD/FTD) characterized by trophoblast necrosis with preserved villous stroma, collapse of the intervillous space, intervillous fibrinoid deposits, and variable polymorphous inflammatory infiltrates. Cases with DTD (>80% of the parenchyma affected) resulted in 5 stillbirth and 1 premature alive baby (27w) born after induction of labor for pathologic fetal non-stress test. In 4/5 deaths an autopsy was performed and infection of fetal tissues was not demonstrated by IHQ. The cases with FTD (<35% of the parenchyma affected) hadn't negative impact on the fetus. Correlation between placental infection and DTD/FTD had statistical significance (p<0,001). 15/16 placentas belonged to the group of pregnant women with active infection within 10 days prior delivery. Correlation between DTD/FTD and maternal active infection had statistical significance (p<0,002).

Conclusions: Placentas infected by SARS-CoV2 has a characteristic histological pattern that we have defined as DTD or FTD, characterized by a predominant villous trophoblast necrosis, intervillous space collapse and variable degrees of mixed inflammation and intervillous fibrinoid deposition. DTD/FTD is an infrequent lesion observed in 5,7% of pregnant women affected by COVID-19 in our series. DTD can be the cause of fetal death due to placental insufficiency. In this study, vertical transmission of the virus to the fetus has not been demonstrated.

1186 Identifying Placental Pathology in Pregnant People Living with HIV Using Machine Learning

Brian Vadasz[1], Lynn Yee[1], Lee Cooper[2], Jeffery Goldstein[1]

[1]Feinberg School of Medicine/Northwestern University, Chicago, IL, [2]Northwestern University, Chicago, IL

Disclosures: Brian Vadasz: None; Lynn Yee: None; Lee Cooper: None; Jeffery Goldstein: None

Background: The placenta is a key driver of diseases of pregnancy and abnormalities in the placenta reflect life-long risk of disease in the mother and infant. Machine learning on scanned whole slide images (WSI) has the potential to decrease interobserver variability and improve reliability of diagnosis. People living with HIV (PLHIV) experience greater risk of adverse birth

outcomes compared to the general population, however the mechanisms are not fully understood. Studies have shown PLHIV have lower placental weight, less circular placentas and have higher rates of abnormal cord insertion. Histopathologic evaluation of HIV placentas has reported significantly increased vascularity and thrombosis. Machine learning could identify quantitative changes and patterns that are not reliably identified by human observers. We aim to identify abnormalities in placenta histology of PLHIV vs individuals without HIV using machine learning.

Design: We have scanned WSI of membrane rolls and full thickness placenta slides from 118 PLHIV and 373 control cases (2010-2020). We compared clinical and histopathologic features between PLHIV and control cases. Our previous work has shown that we were able to successfully develop a placental region identification (ID) classifier that can identify regions of the placenta with an accuracy of 99.1%. We used the region ID algorithm to extract regions of decidua, terminal villi, stem villi, chorion, and amnion from each slide. We will train convolutional neural networks to distinguish HIV vs. non-HIV for each placental region. We will use attention functions, e.g. GRAD-CAM to identify which latent features are used by the algorithm for detection

Results: Gestational age of PLHIV placentas were 37.3+/- 3.3 weeks compared to 38.7+/- 1.9 weeks in the control group (difference of 1.4 weeks, P<0.01). The placental weight in the PLHIV group is 427+/-114 grams compared to 481+/-98 grams in the control group (difference of 54 g, P<0.01). The placental weight controlling for gestational age in our PLHIV group is -0.83+/-1.7 grams compared to -0.46+/-1.22 grams in the control group (difference of 0.37 standard deviations, P<0.01). Persistent muscularization of basal plate arterioles is seen in 14% (17/118) of PLHIV vs. 3.5% (13/373) of controls (OR 6.3, P<0.001). Decidual arteriopathy is seen in 21% (25/118) of PLHIV vs. 7% (26/373) of controls (OR 3.9, P<0.001). Chronic villitis of unknown etiology seen in 6.8% (8/118) vs 23% (85/373) of controls (OR 0.25, P<0.001) (Figure 1).

Figure 1 - 1186

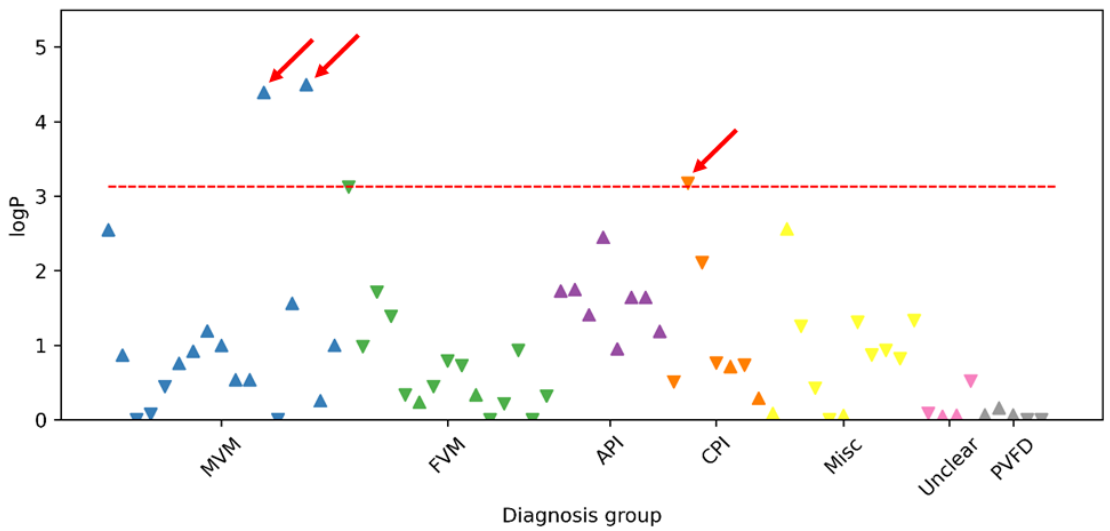

Figure 1. Manhattan plot showing the strength of association between PLHIV and placental diagnoses. Decidual arteriopathy, persistent muscularization of basal plate arterioles, and chronic villitis of unknown etiology (red arrows from left to right) show significant differences in frequency after correcting for multiple corrections (p-value threshold (0.05 / # of comparisons, red dashed line). API: acute placental inflammation; CPI: chronic placental inflammation; FVM: fetal vascular malperfusion; logP: base 10 logarithm of the P-value; Misc: miscellaneous lesions (e.g. basal plate myometrial fibers; MVM: maternal vascular malperfusion; PVFD: lesions involving perivillous fibrin deposition; Unclear: findings of uncertain significance.

Conclusions: We show there are many gross and histopathological differences between placentas from PLHIV compared to people without HIV. Our next steps are to create an algorithm that further classifies and identifies abnormalities within the placenta in PLHIV. In addition, we aim to identify latent features, which may lead to better understanding of the mechanisms of adverse clinical and birth outcomes of PLHIV.